

Copyright © IJCESEN

International Journal of Computational and Experimental Science and ENgineering (IJCESEN)

Vol. 11-No.4 (2025) pp. 7843-7849 http://www.ijcesen.com

Research Article



Effect of temperature on Microstructure and Corrosion Behavior of Carbon Steel: Experimental study and modeling

Fatiha Chelgham^{1,2*}, Khadra Mokadem³, Amira Ouakkaf⁴, Mounira Chelgham⁵, Souheyla Boudjema⁶, Hafsa Daoui⁷, Noureddine Bouzid⁸

¹Laboratoire de Valorisation et Promotion des Ressources Sahariennes, Université Kasdi Merbah, Ouargla - 30000, Algerie.

²Faculté des hydrocarbures, énergies renouvelables, science de la terre et de l'univers, Université Kasdi Merbah, Ouargla-30000, Algerie.

* Corresponding Author Email: fchelgham@gmail.com - ORCID: 0000-0002-5247-9650

³Faculté des hydrocarbures, énergies renouvelables, science de la terre et de l'univers, Université Kasdi Merbah, Ouargla-30000, Algerie.

Email: khadr2a@gmail.com - ORCID: 0000-0002-5247-9550

⁴Faculté des sciences exactes, Université Mohamed Khider, Biskra,07000, Algerie.

Email: amir2a@gmail.com - ORCID: 0000-0002-5247-9450

⁵Développement des énergies nouvelles et renouvelables dans les zones arides et sahariennes, LENREZA, P.O. Box 511, Ouargla 30 000, Algeria

Email: mounir2a@gmail.com - ORCID: 0000-0002-5247-9350

⁶Département de chimie, Laboratoire de catalyse et synthèse en chimie organique, Univesité de Tlemcen, Tlemcen, Algérie.

Email: souheyl2a@gmail.com - ORCID: 0000-0002-5247-9250

⁷Faculté des hydrocarbures, énergies renouvelables, science de la terre et de l'univers, Université Kasdi Merbah, Ouargla-30000, Algerie.

Email: hafs2a@gmail.com - ORCID: 0000-0002-5247-9150

⁸Structures , Properties and Inter Atomic Interactions Laboratory (LASPI2A), Faculty of Science and technology, University of Abbes Laghrour, Khenchela- 40000, Algeria.

Email: noureddin2e@gmail.com - ORCID: 0000-0002-5247-9050

Article Info:

DOI: 10.22399/ijcesen.4161 **Received:** 11 June 2025 **Accepted:** 27 September 2025

Keywords

API N80, tempering temperature, Corrosion, Quadratic Model

Abstract:

Oil field water source wells are vulnerable to corrosion issues because of their intricate operating environments. Because corrosion-related failures result in significant downtime, managing corrosion is a crucial and complicated task in the petroleum and gas industry. This study used X-ray diffraction (XRD), an electrochemical measuring technique, to examine the impact of tempering temperatures (200, 400, and 500 °C) on the corrosion behavior of American Petroleum Institute (API) N80 steel in albian water at various gradient temperatures. The API N80 steel samples crystallize in a ferritetype structure, according to XRD patterns. All of the API N80 samples, we noted, have a nanometric grain size . As the tempering temperature rises, there is a correlation between the corrosion rates of samples and structural changes . Excellent corrosion resistance and a decreased corrosion current density were demonstrated by steel N80 at a higher tempering temperature. Increased grain sizes and decreased residual stress and hardness are the reasons for the corrosion resistance difference. The Quadratic Corrosion Model was used to determine the optimal operating conditions for minimizing the corrosion rate. The statistical model predicted the optimal conditions for the selected t variables as a tempering temperature of approximately 450 °C, and a thermal gradient (ΔT) of around 1 °C, Under these conditions, the predicted corrosion rate is in the range of 37 μm/year.

1. Introduction

The majority of oilfields use water injection as their oilfield development technique in order to maintain or raise the reservoir pressure and achieve a greater recovery rate. The corrosive conveying medium, which comprises a range of corrosive components such carbon dioxide, chloride ions, solid particles, etc., is directly in touch with the inner wall of the water source well [1-2]. The water source well's inner wall is severely eroded as a result of these elements working together. To satisfy the anti-corrosion requirement, standard N80 carbon steel pipe must be replaced on a regular basis.

One of the most used materials in the oil and gas sector is carbon steel. The L80 , J55, P110, and N80 materials are utilized for geothermal well casings or tubing. The materials used for injection well casings, transportation pipelines, and other equipment must be able to withstand corrosion from injected gases and fluids [3-7]. Because of their favorable qualities, ease of manufacture, and comparatively low cost, In the petroleum sector, API N80 is typically utilized as the primary building material for transmission pipelines and downhole tubular systems [8-11]. However, in environments where oil is produced, carbon steels are susceptible to corrosion.

One of the most intriguing operational issues to anticipate and manage is corrosion in gas and oil pipelines. The longer a material is exposed to the environment, the faster it deteriorates. It is also influenced by the base alloy's composition and microstructure as well as environmental factors including temperature, flow, pH, and pressure. The creation of preventive techniques has therefore been actively sought after and is now essential to reducing the expense of corrosion [12-15].

Choosing tempering temperature for steels that are resistant to corrosion is one of the best ways to prevent water source well string corrosion and Materials that are resistant to corrosion like inhibitors.

Many researchers have examined the corrosion resistance of steel following treatments. For example, Junlin Song et al. [16] examined the impact of tempering duration during heat treatment on the microstructure and corrosion resistance of bimetallic composites made of carbon steel and stainless steel (SS). And Junwei Yin et al [17] carried out Potentiodynamic polarization tests were used to examine the corrosion resistance of M390 powder metallurgical martensitic stainless steel at various tempering temperatures.

SiyanWang et al. [18] This research looks into the impact of tempering time on HNMSS pitting corrosion in 3.5 weight percent NaCl solution, the

findings indicated that longer tempering durations led to higher pitting sensitivity.

This study examined the effects of tempering temperature on the microstructures and corrosion resistance of API N80 steel pipelines using experimental observations and the Quadratic Corrosion Model to Optimal Operating Conditions.

2. Material and methods:

2.1. Chemical analysis of water

The findings of the chemical analysis of the water are displayed in Table 1. This is because corrosion is a phenomenon in which the environment's characteristics are crucial to the process. The average values of multiple measurements made on water samples from the well in the Haoud Berkaoui region are consistent with these findings. The analysis's findings indicate that the water is chlorinated and high in bicarbonates and phosphates.

2.2. Instrumentation

Table 2 lists the chemical components of API 5CT N80. Following two hours of heating at a rate of 50°C per minute, the specimens were tempered at various temperatures before being cooled in an oven.

Following these procedures, wet abrasive paper with grit sizes of 400, 600, 800, 1000, and 2000 was used to polish each specimen.

A typical sample of API 5CT N80 was used to create the working electrode, which had a 14 cm2 area. The specimens were then placed within the plastic support.

Potentiostat-galvanostat Type PGZ 301 experimental measures are utilized for electrochemical investigations. They are connected to a PC computer using Volta Master-4 software.

We employ a novel electrochemical cell. There are two coaxial cylinders on the test bench. The first cylinder is made up of a glass tank that measures 30 x 20 x 20 cm and has two holes for the reference electrode to be inserted into saturated KCl calomel. The platinum auxiliary electrode portion is 1 cm².

The second cylinder is made up of a 13 x 11 cm² cylindrical tank with a bottom hole that is positioned in steel to serve as the working electrode.

A heating resistor that was managed by a thermostat was used to heat the filled cylindrical vessel. A digital thermometer is also used to take the temperature ench. The first cylinder is made up of a glass tank that measures 30 x 20 x 20 cm and

has two holes for the reference electrode to be inserted into saturated KCl calomel. The platinum auxiliary electrode portion is 1 cm².

The second cylinder is made up of a 13 x 11 cm² cylindrical tank with a bottom hole that is positioned in steel to serve as the working electrode.

A heating resistor that was managed by a thermostat was used to heat the filled cylindrical vessel. A digital thermometer is also used to take the temperature.

Voltamaster 4 software is used to process the results. It allows for direct readings of the corrosion current and rate using the Tafel straight extrapolation method; a scan rate of 30 mV/min was employed.

3. Results and discussion:

3. 1. X-ray diffraction (XRD) analysis:

Fig..1 show the X-ray diffraction spectra of API N80 steel as delivered and tempered at different temperatures. In each case, four pronounced peaks appear at $2\theta = 44.759^{\circ}$, 64.975° , 82.327° , and 98.921° . They are attributed, respectively, to the (110), (200), (211), and (220) planes of the bodycentered cubic ferrite. No peaks relating to cementite, which has an orthorhombic structure, were detected by XRD, but this does not rule out its existence within the steel (as confirmed by DSC analysis). The precipitates are very small and therefore have no significant diffractive effect. This phenomenon was observed by [3]. The value of the ferrite lattice parameter was found to be (a = 2.867\AA).

Nevertheless, we observe that the API N80 samples do not contain any metallic Fe, Mn, Si, Ni, Mo, Cr, or Cu peaks. The XRD pattern clearly shows the establishment of the ferrite phase and shows no additional phases identified.

3. 2. Effect of tempering temperature on grain size:

The Debye-Scherrer equation (1) is utilized to determine the samples' average grain sizes:

$$D = \frac{0.9 \,\lambda}{\beta \cos \theta} \dots (1)$$

Where; D stands for crystallite diameter, θ for Bragg diffraction angle, β for full width at half-maximum (FWHM),

The average ferritic grain size fluctuation as a function of tempering temperature is depicted in Fig. 2. There was no discernible change in ferrite grain size from the reference state to the asdelivered condition. Actually, the corrosion rate of AISI 304 austenitic steel reduces with increasing

grain size, primarily because of the accumulation of flaws at the grain boundaries, according to a study on the subject done by A.DISCHINO et al. 2002 [5]. In actuality, corrosion decreases as grain size increases because there are fewer barriers.

3. 3. Effect of tempering temperature on grain size:

3. 3. 1. Electrochemical Experiments:

Table 3 displays the findings of the electrochemical kinetic parameters (i corr, E corr, ba, and bc) found in Tafel plots for the API N80 electrode in Albian water for untreated steel at various gradient temperatures and tempering temperatures.

Table 3 demonstrates that the untreated steel's corrosion rates were noticeably higher than the albian water's tempering temperature. This is because its ionic species are aggressive toward untreated steel, which causes the steel to break down.

Because of their strong electronegativity and relatively tiny size, the Cl-ions appear to have a greater detrimental effect than SO2-4, speeding up the steel's rate of disintegration. It should be mentioned that the redox electrochemical processes that cause corrosion were increased by the presence of Cl- and SO2-4 ions [19].

Results of polarization tests for API N 80 specimens at T=0,3,6,9,12, and $16^{\circ}C$ are shown in Fig. 3. indicates that when the tempering temperature rises, corrosion rate values generally decrease. However, steel tends to be less resistant to corrosion as the gradient temperature rises. In other words, changes in the gradient temperature had no effect on the corrosion potential. All of the examined specimens displayed pitting corrosion and poor resistance in the electrochemical tests conducted at various tempering temperatures. Out of all the temperature gradients, the API N80 steel that was tempered at $400 \, ^{\circ}C$ had the best corrosion resistance.

Demonstrate how API N80 steel's corrosion resistance has been greatly enhanced. The corrosion potential increased from -676.3 mv to -565.5 mv, and the corrosion current density decreased from $5,6451\mu\text{A/cm}^2$ to $3.1637\mu\text{A/cm}^2$. However, at 500°C , the corrosion potential dropped to -567.4 mv, and the corrosion current density increased to $4.7198\mu\text{A/cm}^2$.

3. 4. Quadratic Corrosion Model

The Quadratic Corrosion Model is an expression for corrosion rate (V) in a function of temperature difference (ΔT) and temperature (T), to incorporate nonlinear and interaction terms to account for saturation and coupling effects:

In comparison, a more straightforward linear model is:

$$V = 77.7040 + 6.3153 \cdot \Delta T - 0.0249 \cdot T$$
....(3)

The quadratic formulation is suitable when curvature and variable interactions are expected to be shown by experimental data, while the linear formulation may be sufficient for approximations or limited data. Table 4 presents a comparison of the goodness-of-fit metrics for the linear and quadratic models using the existing dataset. The quadratic model (RSM) demonstrated a smaller RMSE (20.19 μ m/y vs. 22.81 μ m/y), a smaller MAE (18.10 μ m/y vs. 19.26 μ m/y), and larger R² (0.7594 vs. 0.6932) values, indicating a better fit with the experimental data. From a practical perspective, since the quadratic model predicts that increasing ΔT will lead to an increase in V, but after a certain point the negative quadratic mean means that the rate becomes constant or decreases (another saturation effect that does not occur with the linear form), it would be reasonable to assume the best fit through the linear model for

evaluations of limited data or for approximate evaluations. The quadratic model would be more useful for operational recommendations, and optimizations if it is applicable in similar conditions as the experimental data.

Each row lists the observed corrosion rate V and the predictions from the Linear OLS and Quadratic models, with absolute and relative errors.

Based on the Figure. 4, the safest and most effective operating region is at a near-zero thermal gradient and a mid-range tempering temperature. The quadratic (nonlinear) surface $V(\Delta T, T \text{ rev})$ predicts its minimum within the tested domain at approximately $\Delta T \approx 0$ °C and T rev ≈ 290 °C, consistent with the experimental valley observed at $\Delta T = 0$ and T rev = 200–400 °C where the lowest measured rates (~37–38 µm/y) occur. The linear model suggests pushing T_rev to the upper bound simply because it is a plane and cannot capture curvature, so it is not recommended for optimization. Practically, we propose a robust setpoint of $\Delta T \approx 0$ °C with T rev = 280–320 °C; if a gradient cannot be eliminated ($\Delta T > 0$), keep T rev $\approx 300-400$ °C and avoid ~ 500 °C, which tends to increase corrosion at higher ΔT .

Table 1. Results of the chemical analysis of Albian water.

Elements	Ca ⁺²	Mg ⁺²	Na ⁺	K ⁺	Cl ⁻	SO_4^{2-}	<i>HCO</i> ₃	NO_3^-	pН
Composition (mg/l)	175. 56	92.82	284.28	33	526.85	561.14	150.14	11.85	7.79

Table 2. The chemical composition of API N80 steel.

Elements %	Fe	С	Mn	Si	Р	S	Ni	Cr	Mo	Cu	V
Composition	98.48	0.21	0.75	0.1	0.007	0.007	0.05	0.12	0.05	0.16	0.01
%											

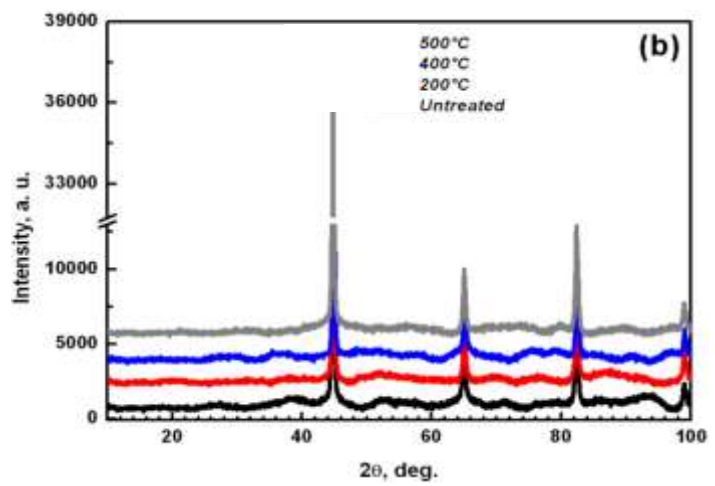


Figure 1: X-ray diffraction spectra of API N80 steel's tempering temperature.

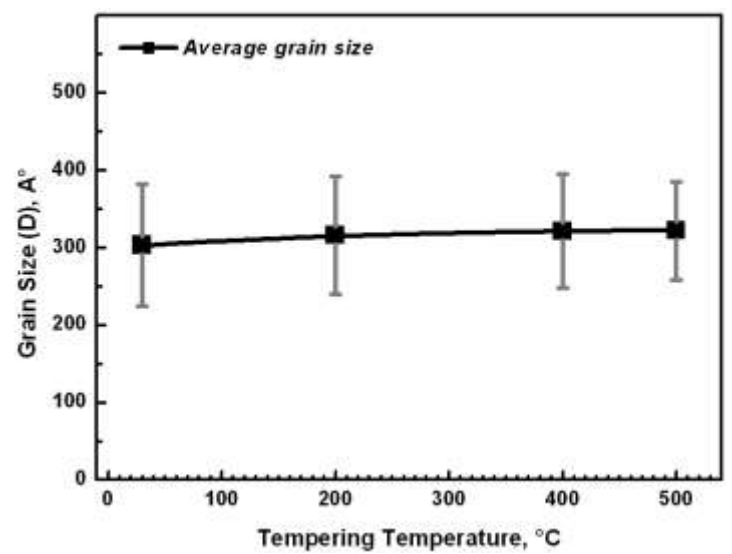


Figure.2. Relationship between average grain size and tempering temperature.

Table 3. Corrosion paraméters at different Gradient temperature for different tempering temperature of steel API N80

Gradient Tempéreature (°C)	Tempering temperature (°C)	Ecorr (mv)	ba (mv/dec)	- bC (mv/dec)	Icorr (μAcm ⁻²)	Corrosion rate V (μm/y)
	untreated	-676,3	74,6	104,6	5,6451	66,02
$\Delta T = 0$	200	-565.5	44.7	163.6	3.1637	37.00
$\Delta 1 - 0$	400	-651.0	53.8	59.7	3.2252	37.72
	500	-567.4	58.8	263.7	4.7198	55.20
	untreated	-691.8	67.4	109.6	10.9596	128.1
	200	-697.4	57.7	88.7	10.1174	118,3
$\Delta T = 3$	400	-692.6	66,7	96,6	9,9807	116,7
A1 0	500	-701.5	64.3	91.3	10.5998	123,9
	untreated	-674.7	74,7	111,6	11,2376	131,4
$\Delta T = 6$	200	-662.1	47.9	62.0	9.3889	109,8
	400	-680,6	49,1	72,3	7,2869	85,23
	500	-686,9	50,7	65,7	8,0118	93,70
	untreated	-681,3	53,4	74,2	11,4212	133,5
$\Delta T = 9$	200	-677,6	50,0	76,6	11,0538	129,2
	400	-680,8	59,0	78,3	9,1917	107,5
	500	-696,1	62,3	80,7	12,1969	142,6
	untreated	-684,2	80,5	112,2	12,7339	148,9
	200	-664,2	54,6	70,0	10,5654	123,5
$\Delta T = 12$	400	-666,9	55,5	89,4	9,2195	107,8
$\Delta 1 - 12$	500	-688,0	71,4	108,9	14,9331	174,6
	untreated	-696,9	76,1	114,7	16,1128	188,4
	200	-696,6	62,3	81,9	15,1511	177,2
$\Delta T = 16$	400	-684,2	77,2	102,1	11,9362	139,6
$\Delta 1 - 10$	500	-689,1	66,7	89,0	15,9677	186,7

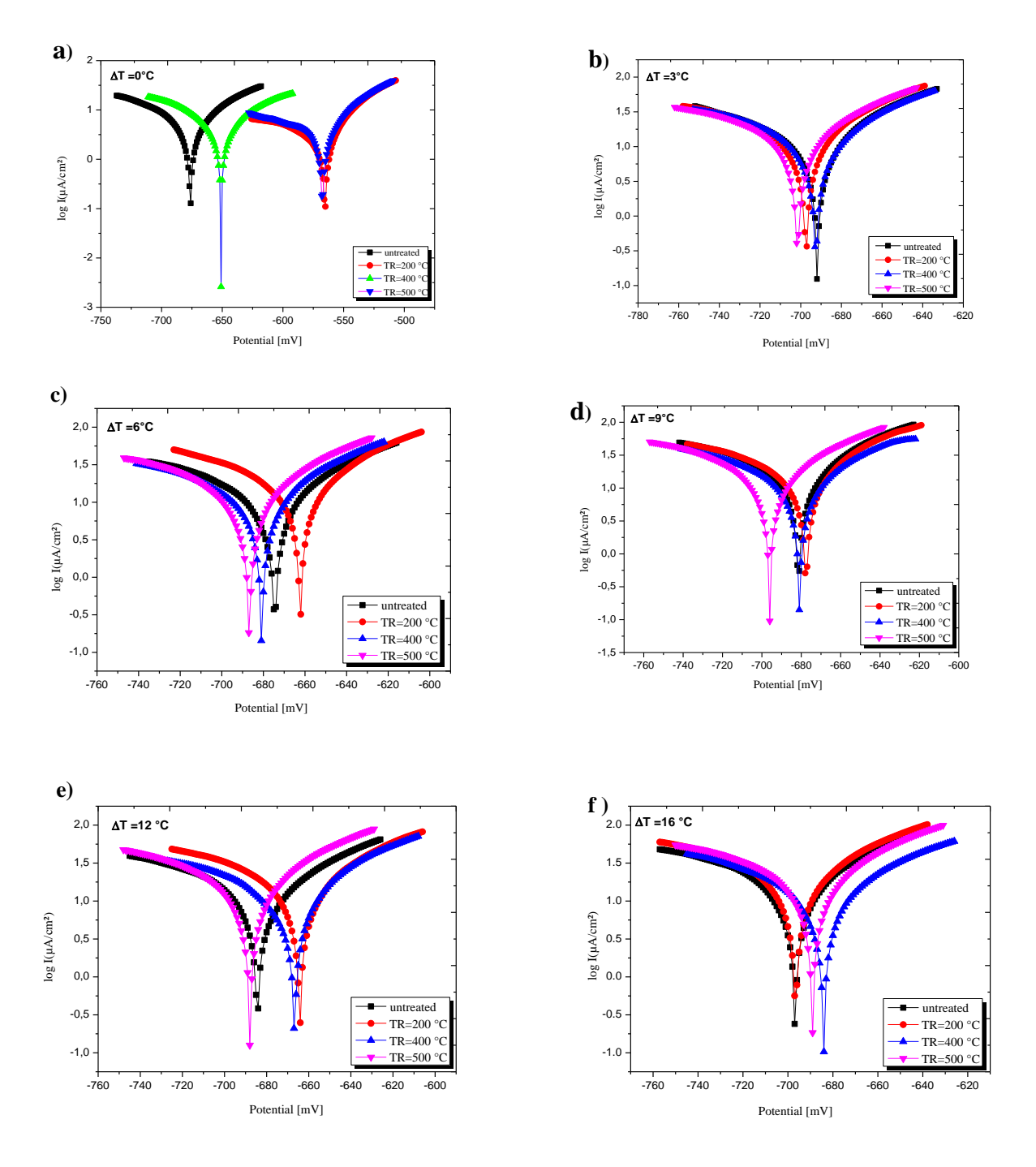


Figure. 3: Results of polarization for various gradients at untreated and tempering temperatures API N80 steel's a) $\Delta T = 0$ °C, b) $\Delta T = 3$ °C, c) $\Delta T = 6$ °C, d) $\Delta T = 9$ °C, e) $\Delta T = 12$ °C, f) $\Delta T = 16$ °C.

 Table 4. Goodness of fit (on provided dataset)

Model	RMSE (μm/y)	MAE (μm/y)	R ²	
Linear (OLS)	22.81	19.26	0.6932	
Quadratic (RSM)	20.19	18.10	0.7594	

Table 5. Iso-Corrosion Rates (Linear and Quadratic Models)

2 West Consistent names (2 west with grant and 12 wests)									
ΔT	T_rev	V_obs	V_pred_l	V_pred_	AbsErr_	RelErr_l	AbsErr_qua	RelErr_q	
(°C)	(°C)	(µm/y)	in (μm/y)	quad (μm/y)	lin (μm/y)	in (%)	d (μm/y)	uad (%)	
0.0	0.0	66.02	77.7	82.58	11.68	17.7	16.56	25.08	
0.0	200.0	37.0	72.72	54.35	35.72	96.55	17.35	46.89	
0.0	400.0	37.72	67.74	55.8	30.02	79.6	18.08	47.94	
0.0	500.0	55.2	65.25	67.66	10.05	18.21	12.46	22.58	

3.0	0.0	128.1	96.65	107.33	31.45	24.55	20.77	16.22
3.0	200.0	118.3	91.67	79.58	26.63	22.51	38.72	32.73
3.0	400.0	116.7	86.69	81.52	30.01	25.72	35.18	30.14
3.0	500.0	123.9	84.2	93.62	39.7	32.04	30.28	24.44
6.0	0.0	131.4	115.6	129.08	15.8	12.03	2.32	1.77
6.0	200.0	109.8	110.62	101.82	0.82	0.74	7.98	7.27
6.0	400.0	85.23	105.64	104.24	20.41	23.94	19.01	22.3
6.0	500.0	93.7	103.15	116.58	9.45	10.08	22.88	24.42
9.0	0.0	133.5	134.54	147.83	1.04	0.78	14.33	10.73
9.0	200.0	129.2	129.56	121.05	0.36	0.28	8.15	6.31
9.0	400.0	107.5	124.58	123.96	17.08	15.89	16.46	15.31
9.0	500.0	142.6	122.09	136.55	20.51	14.38	6.05	4.25
12.0	0.0	148.9	153.49	163.58	4.59	3.08	14.68	9.86
12.0	200.0	123.5	148.51	137.29	25.01	20.25	13.79	11.16
12.0	400.0	107.8	143.53	140.68	35.73	33.14	32.88	30.5
12.0	500.0	174.6	141.04	153.51	33.56	19.22	21.09	12.08
16.0	0.0	188.4	178.75	179.92	9.65	5.12	8.48	4.5
16.0	200.0	177.2	173.77	154.27	3.43	1.94	22.93	12.94
16.0	400.0	139.6	168.79	158.31	29.19	20.91	18.71	13.4
16.0	500.0	186.7	166.3	171.46	20.4	10.93	15.24	8.16

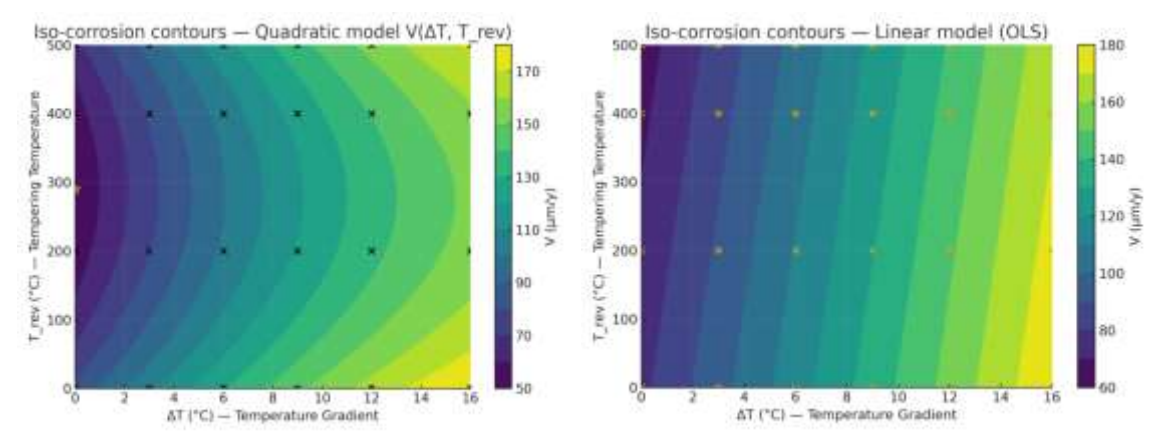


Figure. 4. Iso-Corrosion rate for the Quadratic and Linear Models

4. Conclusions

The XRD and chemical (corrosion) characteristics of steel were examined following tempering at 200, 400, and 500°C. The following is a summary of the study's main findings:

- The API N80 crystallizes in a ferrite-like structure and has nanometric grain sizes in all samples.
- The steel microstructure and resistance to corrosion were significantly impacted by the tempering temperature. Grain size increased as the tempering temperature was raised, indicating a reduction in active sites for corrosion attack and an improvement in the corrosion resistance of the tempered steels;
- The tempering temperature effectively inhibited corrosion in N80 steel in an albian water solution, as evidenced by EIS measurements, which showed a decrease in the corrosion rate:

- Gradient temperature significantly influenced the rate of corrosion in an albian water environment. 16 °C was the temperature at which the corrosion rate peaked.
- Hence, the work established the use fulness of Quadratic Corrosion Model for optimum predicted corrosion rate is in the range.

Author Statements:

- **Ethical approval:** The conducted research is not related to either human or animal use.
- Conflict of interest: The authors declare that they have no known competing financial interests or personal relationships that could have appeared to influence the work reported in this paper
- **Acknowledgement:** The authors declare that they have nobody or no-company to acknowledge.

- **Author contributions:** The authors declare that they have equal right on this paper.
- **Funding information:** The authors declare that there is no funding to be acknowledged.
- **Data availability statement:** The data that support the findings of this study are available on request from the corresponding author. The data are not publicly available due to privacy or ethical restrictions.

References

- Shaban, M. M., Negm, N. A., Farag, R. K., Fadda, A. A., Gomaa, A. E., Farag, A. A., & Migahed, M. A. (2022). Anti-corrosion, antiscalant and antimicrobial performance of some synthesized trimeric cationic imidazolium salts in oilfield applications. Journal of Molecular Liquids, 351, 118610.
- 2. Farh, H. M. H., Seghier, M. E. A. B., & Zayed, T. (2023). A comprehensive review of corrosion protection and control, Engineering Failure Analysis , 143, 106885.
- 3. Papavinasam, S. (2014). Corrosion control in the oil and gas industry (Materials). Elsevier, pp. 133–177.
- 4. Bellarby, J. (2009). Tubing stress analysis. In Well Completion Design, 473–556.
- 5. Wan, R. (2011). Advanced Well Completion Engineering. Gulf Professional Publishing.
- Lopez, D. A., Perez, T., & Simison, S. N. (2003). The influence of microstructure and chemical composition of carbon and low alloy steels in CO2 corrosion: A state-of-the-art appraisal. Materials & Design, 24(8), 561–575.
- 7. Xu, T., Jin, Z., Feng, Y., Song, S., & Wang, D. (2012). Study on the static and dynamic fracture mechanism of different casing-drilling steel grades. Materials Characterization, 67, 1–9.
- 8. Finšgar, M., & Jackson, J. (2014). Application of corrosion inhibitors for steels in acidic media for the oil and gas industry. Corrosion Science, 86, 17–41. https://doi.org/10.1016/j.corsci.2014.04.044
- 9. Yadav, M., Behera, D., & Sharma, U. (2016). Nontoxic corrosion inhibitors for N80 steel in hydrochloric acid. Arabian Journal of Chemistry, 9(2), 1487–1495.
- Vishwanatham, S., & Haldar, N. (2008). Furfuryl alcohol as corrosion inhibitor for N80 steel in hydrochloric acid. Corrosion Science, 50(11), 2999– 3004.
- 11. Zhu, S. D., Fu, A. Q., Miao, J., Yin, Z. F., Zhou, G. S., & Wei, J. F. (2011). Corrosion of N80 carbon steel in oil field formation water containing CO2 in the absence and presence of acetic acid. Corrosion Science, 53(10), 3156–3165.
- 12. Carneiro, J., Tedim, J., & Ferreira. (2015). Chitosan as a smart coating for corrosion protection of aluminum alloy 2024. Progress in Organic Coatings, 89, 348–356. https://doi.org/10.1016/j.porgcoat.2015.03.008
- 13. Finšgar, M., & Jackson, J. (2014). Application of corrosion inhibitors for steels in acidic media for the

- oil and gas industry. Corrosion Science, 86, 17–41. https://doi.org/10.1016/j.corsci.2014.04.044
- 14. Vazirinasab, E., Jafari, R., & Momen, G. (2017). Evaluation of atmospheric-pressure plasma parameters to achieve superhydrophobic and self-cleaning HTV silicone rubber surfaces via a single-step, eco-friendly approach. Surface and Coatings Technology, 341, 40–56. https://doi.org/10.1016/j.surfcoat.2019.07.005
- 15. Chafai, N., Chafaa, S., & Benbouguerra, K. (2017). Synthesis, characterization and the inhibition activity of a new α-aminophosphonic derivative on the corrosion of XC48 carbon steel in 0.5 M H2SO4: Experimental and theoretical studies. Journal of the Taiwan Institute of Chemical Engineers, 70, 331–344. https://doi.org/10.1016/j.jtice.2016.10.026
- Song, J., Gao, Z., Guo, M., Liu, Z., Lv, C., & Hu, W. (2025). Effect of tempering time on the microstructure and corrosion resistance of carbon steel/stainless steel bimetallic composites. Anti-Corrosion Methods and Materials, 72(5), 743–751. https://doi.org/10.1108/ACMM-03-2025-320
- 17. Yin, J., Gu, J., Lin, P., Li, X., Liao, J., & Zhou, J. (2024). The effect of tempering temperature on microstructure and corrosion resistance of M390 powder metallurgical martensitic stainless steel. Heliyon, 10, e36521. https://doi.org/10.1016/j.heliyon.2024.e36521
- Wang, S., Du, H., Shi, Z., Zhang, L., Liu, C., Yan, Z., Wang, J., Wang, C., Cao, W., & Liang, M. (2025). The mechanisms underlying the effect of tempering time on the pitting behavior of high-nitrogen martensitic stainless steel. Corrosion Science, 246, 112748.
- 19. Loto, R. T., Aiguwurhuo, O., & Evana, U. (2016). Corrosion resistance study of heat treated 420 martensitic stainless steel and 316 austenitic stainless steel in dilute acid concentrations. Revista Técnica de la Facultad de Ingeniería Universidad del Zulia, 39(7), 35–40.